Check for updates

Received: 23 December 2022 | Revised: 20 March 2023 | Accepted: 21 March 2023

DOI: 10.1002/esp.5584

CASE STUDY

ESPL WILEY

Geophysical surveys for non-invasive characterization of sinkhole phenomena: A case study of Murisengo

Sabrina Maria Rita Bonetto[1] | Chiara Caselle[1] | Cesare Comina[1] | Federico Vagnon[2]

[1]Department of Earth Science, University of Turin, Torino, Italy

[2]Department of Environment, Land and Infrastructure Engineering, Polytechnic of Turin, Torino, Italy

Correspondence
Chiara Caselle, Department of Earth Science, University of Turin, via Valperga Caluso 35, 10125 Torino, Italy.
Email: chiara.caselle@unito.it

Abstract

The present research investigates the morphology and genetical mechanism of a sinkhole which occurred in 2019 in Murisengo (NW Italy). This landform is representative of several subsidence phenomena that often concern the Monferrato area (NW Italy). In concomitance with the appearance of the sinkhole at the surface, a cone of detrital material was found in the drifts of a nearby underground quarry. A geological survey was performed in the underground quarry in order to understand the interaction between the geological and geostructural features of the rock body and the generation of the sinkhole. Moreover, the underground sinkhole morphology was investigated through electrical resistivity tomography (ERT) surveys performed at the surface. The ERT outputs were combined to obtain a 3D image of the phenomenon and the 3D reconstruction was then compared with the geomorphological and structural setting of the area. Results suggest that a viscoplastic flow of clay-rich sediments within a conduit in the gypsum bedrock (suffusion process) generated the sinkhole.

KEYWORDS
electrical tomography, ERT, geophysical survey, gypsum terrain, sinkhole, underground quarry

1 | INTRODUCTION

Geological areas consisting of highly soluble rocks (e.g., evaporites or carbonates) often develop karst-related morphologies (e.g., caves or long conduits in the underground and sinkholes or dolines at the surface) that may pose multiple hazards. These phenomena need to be addressed through specific investigation methods for risk mitigation, taking into account the peculiarities of karst settings (De Waele et al., 2011; Gutiérrez et al., 2014; Parise, 2010). Karst-related phenomena are often directly or indirectly induced by anthropogenic activities. The increase in human occupation of karst terrains and the frequent increase of hazards caused by anthropogenic alterations result in scenarios of continuously rising impacts and risk (De Waele et al., 2011). National and local authorities are becoming increasingly aware of the sinkhole hazard, and therefore promote risk-assessment campaigns based on multiple techniques (Argentieri et al., 2015).

Risk scenarios may be exacerbated in cases of interference with underground tunnels for civil or mining purposes (Coli et al., 2020). The intersection of underground drifts with karst morphologies may result in unexpected incidents, damages and environmental consequences such as depletion of water resources, permanent lowering of the water table, extinction of local springs and subsidence phenomena at the surface (Golian et al., 2021; Milanovic, 2002). Case histories from around the world have been detailed and described by many authors (e.g., Bonetto et al., 2008; Clay & Takacs, 1997; Coli et al., 2020; Day, 2004; Golian et al., 2021; Hou et al., 2016).

The most common type of surface subsidence morphology in karst areas is the sinkhole. Subsidence sinkholes have a typical subcircular shape, diameters up to hundreds of metres and depths ranging from a few metres to tens of metres. They commonly occur in evaporites, due to their high solubility and low mechanical strength (Gökkaya et al., 2021; Gutiérrez, Cooper, Johnson 2008), and less often in carbonates (De Waele et al., 2011). The weakening effect of water on the strength and rheology of evaporite rocks – usually more significant than on carbonates (Caselle et al., 2022) – additionally increases the hazard of these phenomena in evaporite contexts.

This is an open access article under the terms of the Creative Commons Attribution License, which permits use, distribution and reproduction in any medium, provided the original work is properly cited.
© 2023 The Authors. *Earth Surface Processes and Landforms* published by John Wiley & Sons Ltd.

Subsidence sinkholes in evaporite subsoils can be classified on the basis of the material involved (cover, bedrock or caprock) and the dominant process (collapse, suffusion or sagging) (Gutiérrez, Guerrero, Lucha 2008, 2014). In particular, the processes can be defined as follows:

- *Sagging*. The gradual settlement of the overlying cover by passive sagging or bending.
- *Suffusion*. Depending on the features of the cover sediments (granular or cohesive), this may consist in a progressive downwashing transport of the cohesionless cover or in a downward migration of clay-rich sediments as a viscoplastic flow. In general, cover suffusion sinkholes do not form catastrophically, but gradually, and have funnel- or bowl-shaped geometries, with typical diameters of a few metres.
- *Collapse*. This develops when the cover consists of cohesive deposits with brittle rheology. It describes a progressive upwards migration of an initial arched cavity over the karst conduit. When the upwards collapse of the cavity roof intercepts the ground surface, the sinkhole is abruptly created. In this case, sinkholes may develop over dissolution pipes of relatively small diameter located at very high depths (e.g., karst conduits 60 m deep and <1 m wide).

The characteristics of sinkhole genesis and evolution (e.g., velocity of phenomenon propagation) are strictly related to geological and hydrogeological settings and to anthropic interactions (if any). A deep knowledge of these aspects therefore provides useful information for risk assessment and mitigation in a specific area.

In recent years, many methods for sinkhole risk mitigation have been developed, including: (i) methods that use subsurface sensors (e.g., conventional seismic stations, nano-seismic monitoring, borehole extensometers and reflectometry techniques; Dahm et al., 2011; Gutiérrez et al., 2019; Land, 2013); (ii) remote sensing methodologies (e.g., radar interferometry for the evaluation of subsidence rates, airborne laser scanning and photogrammetry; Galve et al., 2011; Gutiérrez et al., 2019); (iii) methods that use apparatus in direct contact with the ground surface (e.g., trenching for the precise delimitation of specific sinkholes, ground-based interferometric measures, high-precision topographic profiling, Differential Global Navigation Satellite System or Differential Global Positioning System [DGNSS or DGPS], terrestrial laser scanning, measures with tiltmeters; Galve et al., 2011; Gutiérrez et al., 2019); (iv) geomorphological approaches and GIS-based large-scale mapping (Cahalan & Milewski, 2018; Nam et al., 2020; Perrin et al., 2015; Zumpano et al., 2019); (v) predictive stability charts developed on the basis of finite or discrete element modelling (FEM or DEM) or laboratory experiments based on equivalent physical models (Al-Halbouni et al., 2019; Goodings & Abdulla, 2002; Jia et al., 2018; Luu et al., 2019; Perrotti et al., 2019; Xiao et al., 2020).

Geophysical approaches have also been used as alternative methods of investigation, with the advantage of reducing uncertainties related to superficial anthropogenic or natural modifications (Argentieri et al., 2015; Youssef et al., 2020). The material contrast between the sinkhole sediments and host rock (e.g., density, electrical resistivity, electrical permittivity) makes it possible to identify limits and underground geometries of pre-existing karst, even in the absence of surface evidence (e.g., Kaufmann et al., 2014; Varnavina et al., 2019).

However, geophysical results are strongly dependent on the particular features associated with karst processes, such as sinkhole fillings, decompaction of underground materials, water table changes, denser vegetation growth and/or structural and geometrical changes of the underground units affected by cavity propagation (e.g., Pueyo Anchuela et al., 2015).

Among the geophysical techniques available, electrical resistivity tomographies (ERTs) have often provided reliable results with the advantages of reduced costs and processing time. In particular, the boundary between host rock and sinkhole material can often be identified as high- or low-resistive sectors, as a consequence of the presence of water, clay-rich sediments and/or fractured and loose rock (with high-resistive anomalies if fissures are air filled or low resistive if they are water/clay filled). Nevertheless, the usefulness of the ERT technique must be evaluated case by case, also in relation to the genetical sinkhole process, the expected features of sinkhole materials and the features of the host rock.

Due to the presence of huge volumes of Messinian gypsum and evaporite sediments, the area of Monferrato (Piedmont Region, NW Italy) is susceptible to subsidence, collapses and surface karst events (Banzato et al., 2017; Bonetto et al., 2008; Vigna et al., 2010, 2017). Moreover, many gypsum quarries are located in the area and some of these phenomena might be associated with gypsum exploitation. In this paper, we present the results obtained from fieldwork performed around a sinkhole that occurred during spring 2019 in the municipality of Murisengo (Monferrato area, Piedmont Region, NW Italy). The phenomenon was investigated through a geological survey in the drifts of a nearby underground gypsum quarry (Murisengo quarry) and by performing five ERTs from the surface in the area close to the sinkhole. Direct underground observations in the drifts made it possible to validate the indirect measurements performed from the surface. The results of geophysical surveys and field observations were interpreted and discussed with the aim of defining the genetical model and identifying the possible causes that drove the generation of the sinkhole.

2 | CASE STUDY: THE 2019 MURISENGO SINKHOLE

The underground quarry of Murisengo (Figure 1a) is sited in the Monferrato area (Piedmont Region, NW Italy), characterized by large volumes of Messinian evaporite units. More specifically, in close proximity to the Murisengo quarry, the evaporite sediments are organized in a several-kilometre chaotic rock unit denominated the Valle Versa Chaotic Complex (Figure 1b). This chaotic unit was deposited during a late phase of the Messinian Salinity Crisis, when part of the previously deposited evaporite sediments were involved in large-scale mass gravitative events, triggered by the intra-Messinian tectonic activity. In the study area, this tectonic activity is mainly identified by a NW–SE transpressive fault (Villadeati Fault; Dela Pierre et al., 2003) that separates Oligocene to middle Miocene sediments in the NE part of the area from the Messinian to Pliocene sedimentary sequence outcropping in the SW (Figure 1b).

The Valle Versa Chaotic Complex is organized in blocks of gypsum and carbonate rocks embedded in a fine-grained matrix. The gypsum blocks that reproduce the facies variability of the primary units (e.g., massive selenite, banded selenite, branching selenite, gyps-rudite and gyps-arenite) have maximum sizes of hundreds of metres (Dela

10969837, 0, Downloaded from https://onlinelibrary.wiley.com/doi/10.1002/esp.5584 by CochraneItalia, Wiley Online Library on [07/05/2023]. See the Terms and Conditions (https://onlinelibrary.wiley.com/terms-and-conditions) on Wiley Online Library for rules of use; OA articles are governed by the applicable Creative Commons License

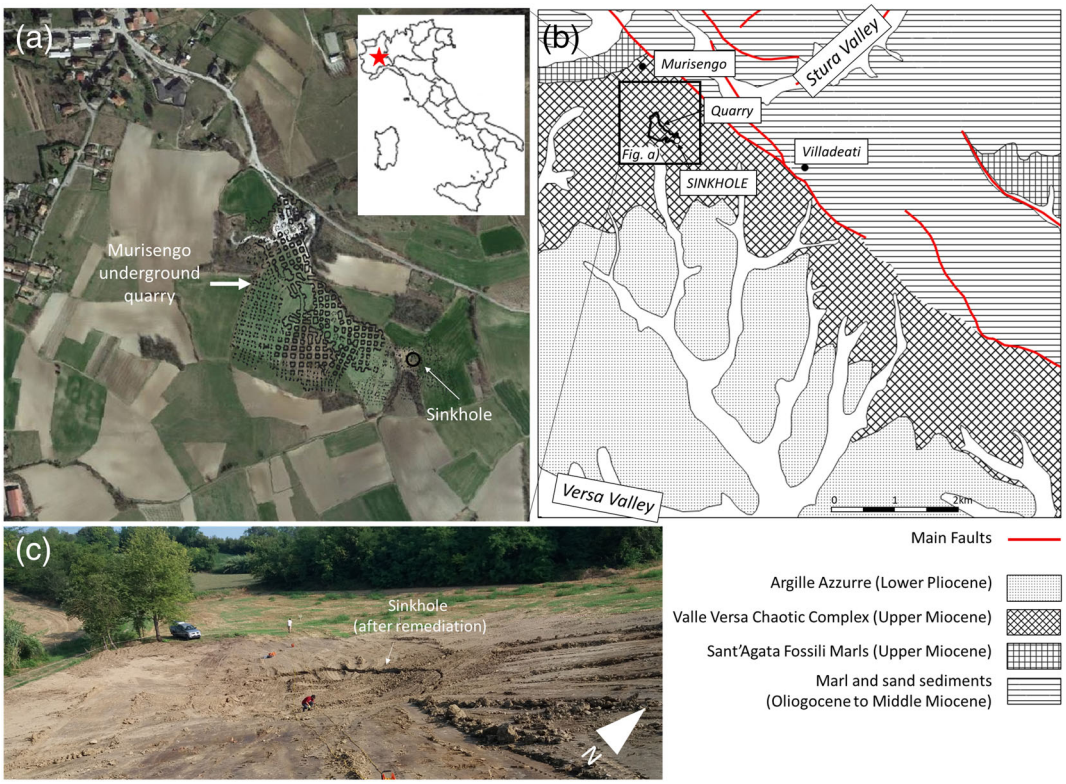

FIGURE 1 (a) Location, (b) geological sketch of the study area and (c) photograph of the 2019 Murisengo sinkhole (after remediation).

Pierre et al., 2016). From a geomechanical point of view, the Valle Versa Complex can be considered as a block-in-matrix formation (or bimrock), with a matrix of silty muds enclosing millimetre- to micrometre-sized clasts of Messinian and pre-Messinian units.

The Murisengo quarry is organized in six underground layers (drifts A to E, shown in Figure 6, and drift F, at a greater depth). A drill-and-blast excavation method is adopted here, with a resulting room-and-square-pillar exploitation scheme. The cover sediments that overlay the gypsum orebody are mainly clay-rich deposits with a non-uniform thickness.

During spring 2019, after long and heavy rains, a sinkhole developed on the ground surface, at an altitude of ~237 m a.s.l. (Figure 1c). The sinkhole had an average diameter of ~20 m and a maximum depth of ~1.5 m.

3 | MATERIAL AND METHODS: GEOLOGICAL AND GEOPHYSICAL SURVEYS

After the sinkhole was revealed on the surface, dedicated geological surveys were planned in the underground tunnels of the quarry. In particular, the inspections focused on the description of geological and geostructural features of the rock mass and on the census of detrital material in the underground tunnels.

During August 2019 and February 2020, moreover, two geophysical (ERT) campaigns were conducted from the ground surface, near the sinkhole area. In particular, five ERT profiles (Figure 2) were acquired with a Syscal-Pro (Iris Instruments) resistivity metre using a Wenner–Schulumberger quadrupole configuration. Acquired data were first filtered by removing bad datum points and then inverted with Res2DInv software (Loke, 2010), applying the least-squares method. Coordinates and elevations of each electrode were taken with a handheld GPS and included in the inversion process. Length and acquisition parameters of each ERT profile are summarized in Table 1.

The two ERT profiles performed in August 2019 (Profiles 1a and 2a in Figure 2) were centred on the sinkhole and designed to ensure a satisfyingly lateral resolution and a sufficient depth of investigation for defining the sinkhole volume. The February 2020 survey (Profiles 1g, 2g and 3g in Figure 2) was designed for evaluating possible interactions between the sinkhole surface evidence, the deeper gypsum orebody and the quarry drifts.

4 | RESULTS

4.1 | Geological survey in the underground drifts

The underground observations confirmed the block-in-matrix organization of the rock mass. The rock blocks mainly consist of gypsum in different facies (e.g., massive selenite, banded selenite, branching selenite and gyps-rudite). The block size ranges between a few centimetres and several tens of metres (Figure 3b). Blocks may be directly in contact with other blocks, creating areas with a predominant clast-supported structure (Figure 3a), or separated by the mud-breccia that represents the matrix of the chaotic rock mass ('matrix-supported structure', Figure 3b).

The rock mass is crossed by several discontinuities, including (i) stratigraphic surfaces, mainly associated with the primary stratigraphic contact between massive layers of gypsum and layers of marl

10969837, 0, Downloaded from https://onlinelibrary.wiley.com/doi/10.1002/esp.5584 by CochraneItalia, Wiley Online Library on [07/05/2023]. See the Terms and Conditions (https://onlinelibrary.wiley.com/terms-and-conditions) on Wiley Online Library for rules of use; OA articles are governed by the applicable Creative Commons License

FIGURE 2 ERT profiles performed during August 2019 (Profiles 1a and 2a) and February 2020 (Profiles 1g to 3g).

TABLE 1 ERT profile characteristics.

Name	No. electrodes	Spacing [m]	Total length [m]	No. measurements	Date of survey
Profile 1a	72	2	142	1287	August 2019
Profile 2a	72	2	142	1287	August 2019
Profile 1g	72	5	355	1287	February 2020
Profile 2g	72	5	355	1287	February 2020
Profile 3g	72	5	355	1287	February 2020

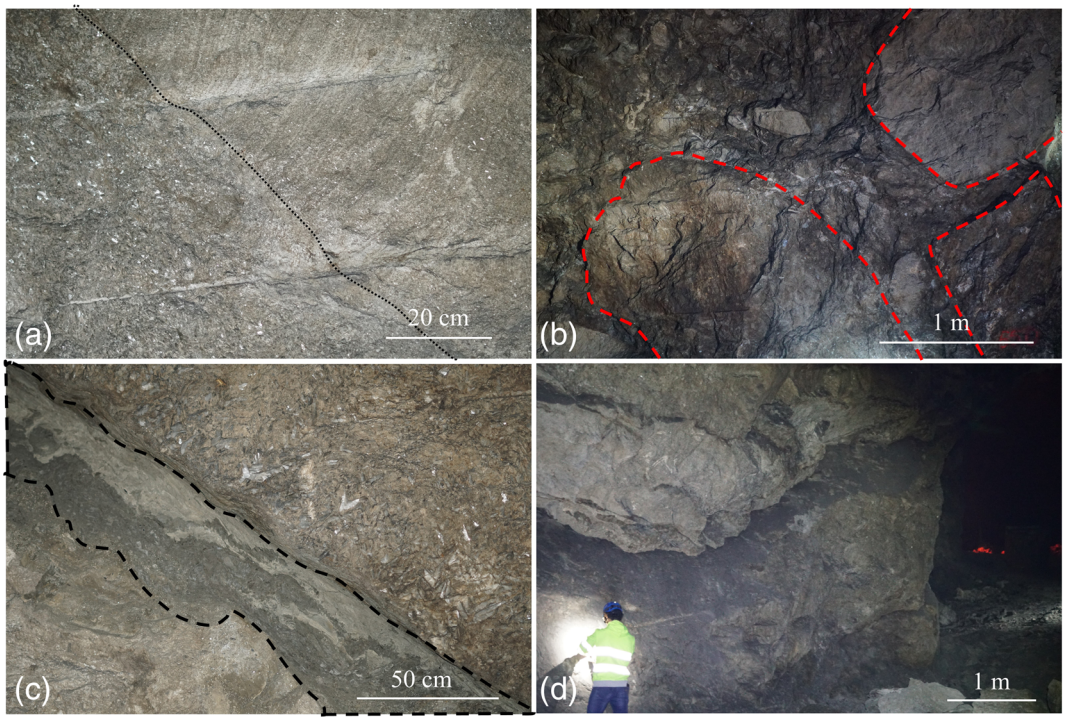

FIGURE 3 (a) Contact between two gypsum blocks (black dashed line). The two blocks are respectively in massive selenite facies (below the line) and in banded gypsum facies (above the line). (b) Blocks of gypsum within a mud-breccia that represents the matrix of the chaotic rock unit. (c) Example of stratigraphic discontinuity, with a layer of marl (black dashed line) in primary contact with the upper volume of massive selenite gypsum (regularly oriented 'arrow head' gypsum crystals are clearly visible). (d) Example of mechanical discontinuity surface, represented by a fault surface (with evidence of strike-slip lineation).

10969837, 0, Downloaded from https://onlinelibrary.wiley.com/doi/10.1002/esp.5584 by CochraneItalia, Wiley Online Library on [07/05/2023]. See the Terms and Conditions (https://onlinelibrary.wiley.com/terms-and-conditions) on Wiley Online Library for rules of use; OA articles are governed by the applicable Creative Commons License

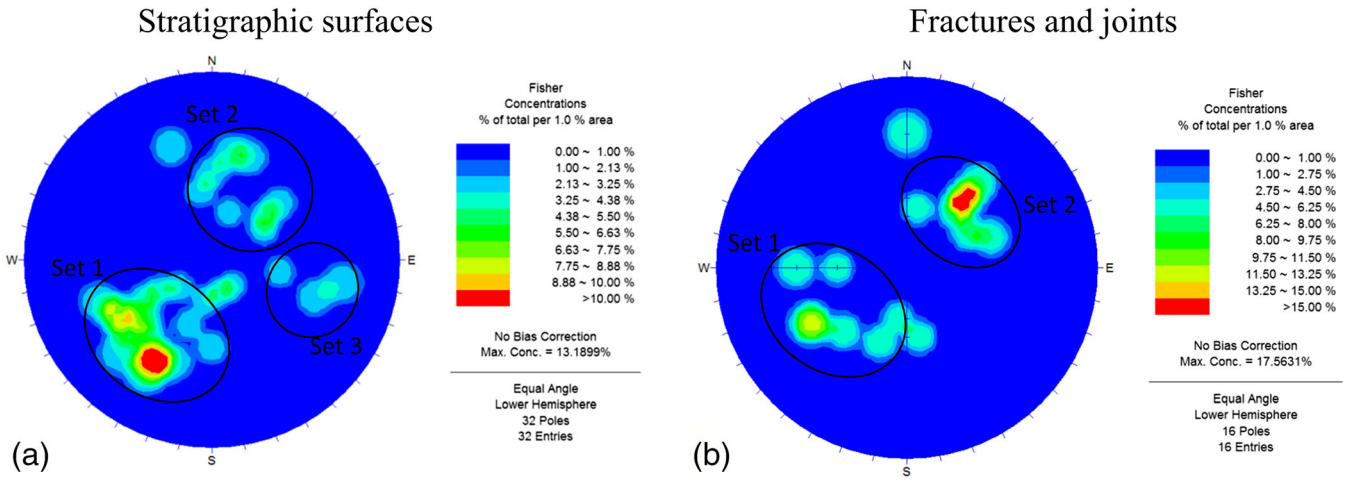

FIGURE 4 Plot of stratigraphic (a) and mechanical (b) discontinuity surfaces measured in the underground quarry.

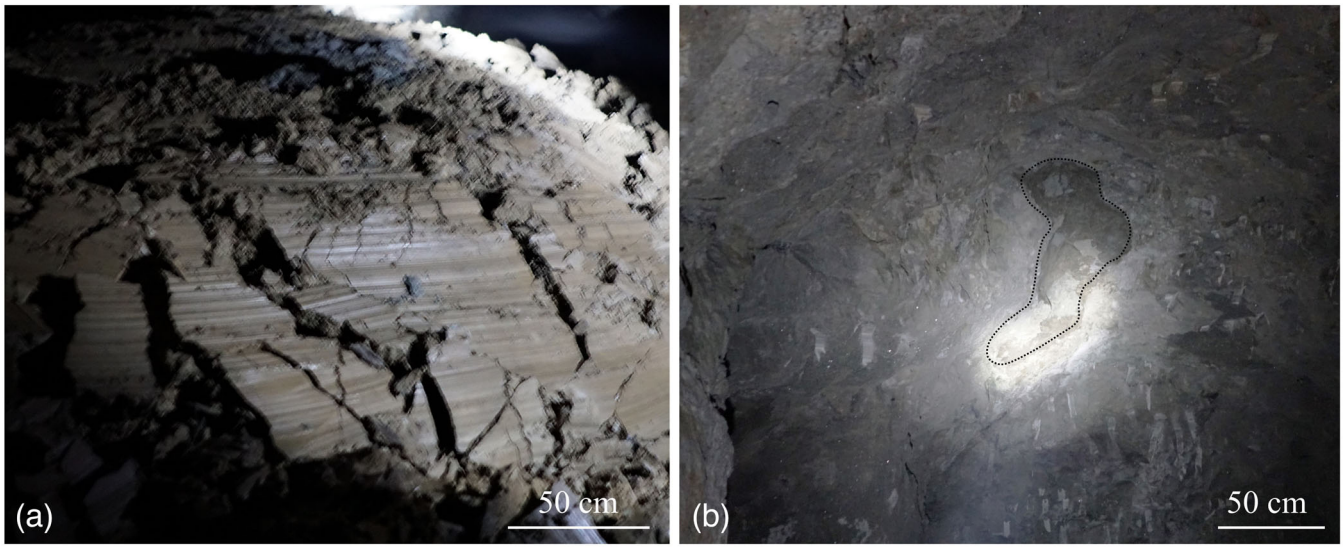

FIGURE 5 (a) Cone of detrital material found in the underground tunnel D of the quarry. (b) Clay chip on the roof of tunnel D near the detrital cone.

(e.g., Figure 3c) and (ii) joints and faults, represented by fragile structures that often show the presence of strike-slip striae (e.g., Figure 3d). Along these surfaces, the presence of filling material consisting of mud-breccia is commonly observed. A census of the most relevant discontinuities (Figure 4) highlights that both stratigraphic surfaces and joints and faults have prevalent NW–SE direction and dip angles ranging between 30 and 70°. In particular, most of the stratigraphic discontinuities dip towards the NE (Set1 in Figure 4a).

During the underground observations, a big volume of detrital material was found in a drift sited between altitudes 188 m a.s.l. (floor) and 195 m a.s.l. (roof) (i.e., at a depth of >40 m from the sinkhole at the surface [~237 m a.s.l.]). This material was located towards the end of the drift at a distance of ~120 m NW from the surface sinkhole.

The observed material consists of a detrital cone of ~2000 m^3 of brown clay-rich sediments (Figure 5a). This material has similar characteristics to the surface soil and appears not completely disarticulated, still maintaining some coherence. Its surface is characterized by the presence of lineation structures that underline a slip displacement (Figure 5a).

This cone was found below a little open conduit in the tunnel roof. In general, the rock mass in this part of the quarry shows a predominant presence of matrix, in spite of more distant and disperse gypsum blocks (situation exemplified in Figure 3b). The matrix is highly heterogeneous and is characterized by the frequent presence of clay chips and other extraneous bodies (Figure 5b).

4.2 | Geophysical survey

Figure 6 shows the inverted ERT profiles acquired in the field during the 2019 and 2020 surveys. A good convergence of the inversions was obtained for all the investigated profiles, with root mean square (r.m.s.) values always <7%.

10969837, 0, Downloaded from https://onlinelibrary.wiley.com/doi/10.1002/esp.5584 by CochraneItalia, Wiley Online Library on [07/05/2023]. See the Terms and Conditions (https://onlinelibrary.wiley.com/terms-and-conditions) on Wiley Online Library for rules of use; OA articles are governed by the applicable Creative Commons License

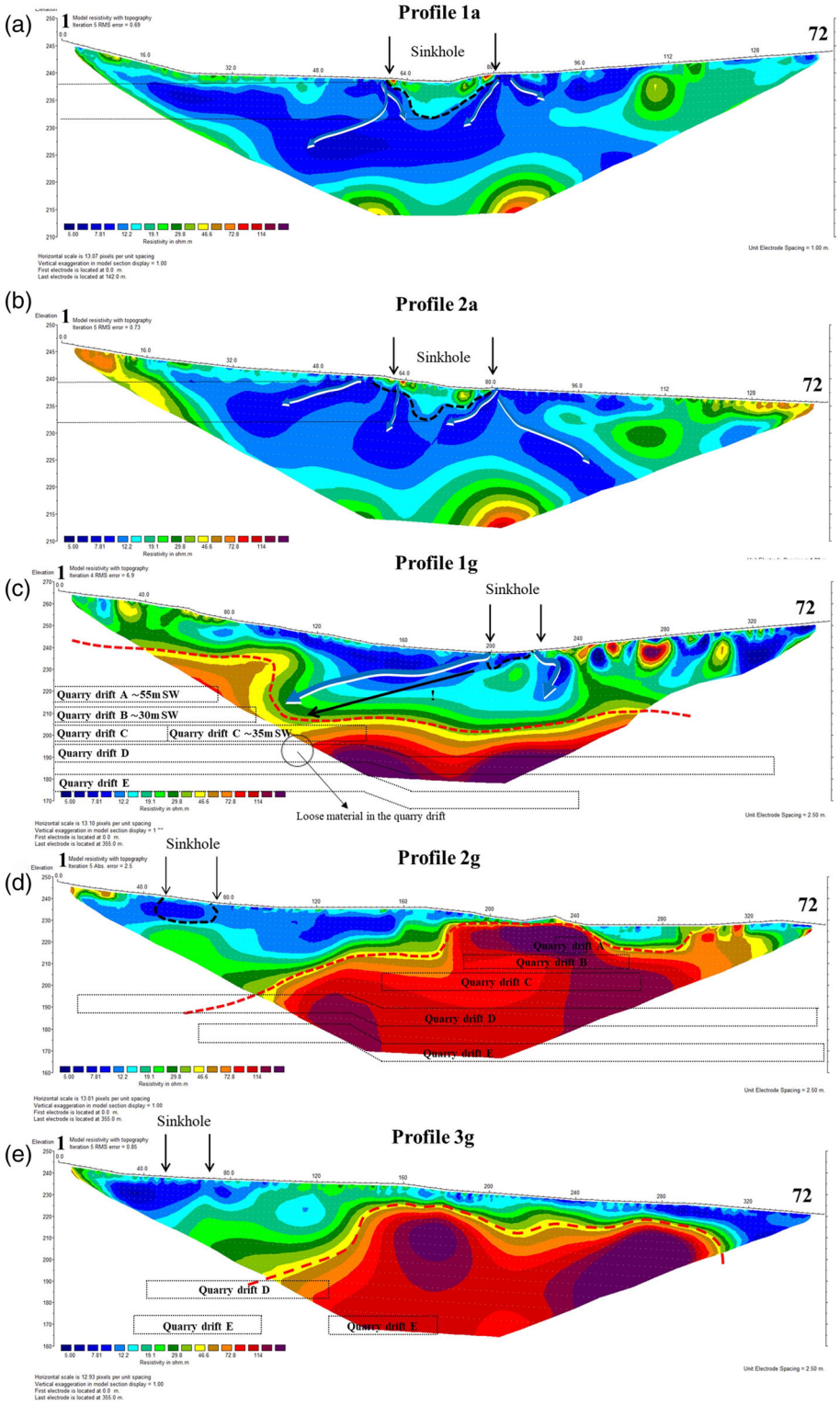

FIGURE 6 Inverted ERT profiles performed and interaction with underground quarry.

The five profiles show the presence of a superficial layer with low resistivity values (≤5–20 Ωm) over a layer with higher resistivity values (>70 Ωm) that respectively represent the clay-rich cover and the gypsum orebody. The limit between these two layers ranges between a few metres and 30–40 m of depth (red dashed line in Profiles 1g, 2g and 3g in Figures 6c–e). The irregular shape of this limit is consistent with the chaotic nature of the orebody that, as explained in the previous paragraphs, consists in the juxtaposition of gypsum blocks with sizes up to hundreds of metres.

Profiles 1a and 2a (Figures 6a and b) show, in correspondence with the surface morphology of the sinkhole, an area with higher resistivity values (15–20 Ωm; black dashed line in Figures 6a and b) surrounded by materials with lower resistivity values (<10 Ωm). This area, which has a conical shape and mean depth of 13–14 m from the surface, represents the weathered, disjointed and porous soil of the sinkhole.

Despite the differences in spatial resolution and acquisition depth, all the ERT profiles show, within the superficial cover layer, the presence of sectors with very low resistivity (<10 Ωm) that propagate

10969837, 0, Downloaded from https://onlinelibrary.wiley.com/doi/10.1002/esp.5584 by CochraneItalia, Wiley Online Library on [07/05/2023]. See the Terms and Conditions (https://onlinelibrary.wiley.com/terms-and-conditions) on Wiley Online Library for rules of use; OA articles are governed by the applicable Creative Commons License

from the sinkhole to the gypsum orebody in the NW direction (light blue arrows in Figures 6a–c). These sectors represent soils with high hydraulic conductivity and (probably) high saturation degree that might be associated with potential flow paths, in agreement with the superficial topographical evidence and the presence of material in the underground drifts of the quarry.

5 | DISCUSSION

Following the geomorphological sinkhole classification developed by Gutiérrez, Guerrero, Lucha (2008, 2014), we propose an interpretation of the Murisengo sinkhole based on the cover suffusion genetic model (Figure 7). As explained and discussed in the previous paragraphs, the initial geological context is represented by an irregular gypsum body, consisting of big blocks differently oriented and separated by a fine-grained gypsum-rich matrix (i.e., the Valle Versa Chaotic Complex), overlaid by a clay-rich cover up to the ground surface (Figure 7a). This initial geological context is further perturbated by the presence of an underground infrastructure (i.e., quarry tunnels). Due to the heterogeneity of the rock mass in terms of material strength and competence, the disturbance created by the quarry is not uniform throughout the tunnels' extension. In addition, as observed by the ERTs, the contact between the gypsum rock mass and the cover sediments is strongly irregular in consequence of the block-in-matrix organization of the orebody. The irregular geometry of the gypsum-cover contact implies that the quarry tunnels are separated by the clay-rich cover material by a random and unpredictable thickness of rock. A potential interference between the underground tunnels and the surfaces will be more probable in the portions with the thinnest rock mass septum between drifts and cover material and/or in the portions with a prevalently matrix-supported rock mass.

Following the proposed interpretation, the process is triggered by water infiltration in the covering soil. The presence of a topographical depression in the area where the sinkhole occurred concurs with the increase of water accumulation at the surface and infiltration in the sediments (Figure 7a), inducing an internal erosion that generates some preferential paths within the sediments, until the evaporitic deposit (Figure 7b). Due to the irregularity of the gypsum-cover contact, the water tends to concentrate in correspondence with a natural depression of the roof of the gypsum body. This brings it to the opening of a karst conduit (and/or to the infiltration of water along permeability contrasts between gypsum blocks and matrix). Here, the thickness of the gypsum septum at the top of the quarry drifts has its minimum thickness. Hence, the conduit reaches the drifts (Figure 7c). The further contribution of meteorological water eventually saturates the clay-rich cover sediments that slowly flow through the karst conduit (Figure 7d).

The features of the detrital cone found in the quarry drifts (not completely disarticulated and with evidence of strike lines; see Figure 5) are consistent with the proposed explanation. Furthermore, the 3D imaging of ERT profiles (Figure 8) add new elements in supporting this hypothesis.

In Figure 8a, the yellow surface represents the tridimensional reconstruction of the contact between gypsum bedrock and clay-rich sedimentary cover (i.e., the electrical resistivity isosurface that corresponds to the red dashed line in Figure 6). The upper limit of the gypsum body has a main dip direction towards the NE (red square in Figure 8a). This NE-dipping orientation that brings the gypsum to outcrop in the SW portion of the survey area (as represented by the hole in the yellow isosurface) is consistent with the mean orientation of stratigraphical and structural surfaces measured in the site (Figure 4) and with the mean orientation of the main regional tectonic structures (Villadeati structure, Figure 1b).

Figure 8 also shows the presence of a structure in the upper surface of the gypsum chaotic formation that dips towards the NW (blue oval in Figures 8a and b). A NW-dipping orientation is consistent with the third set of discontinuities identified in the plot in Figure 6a.

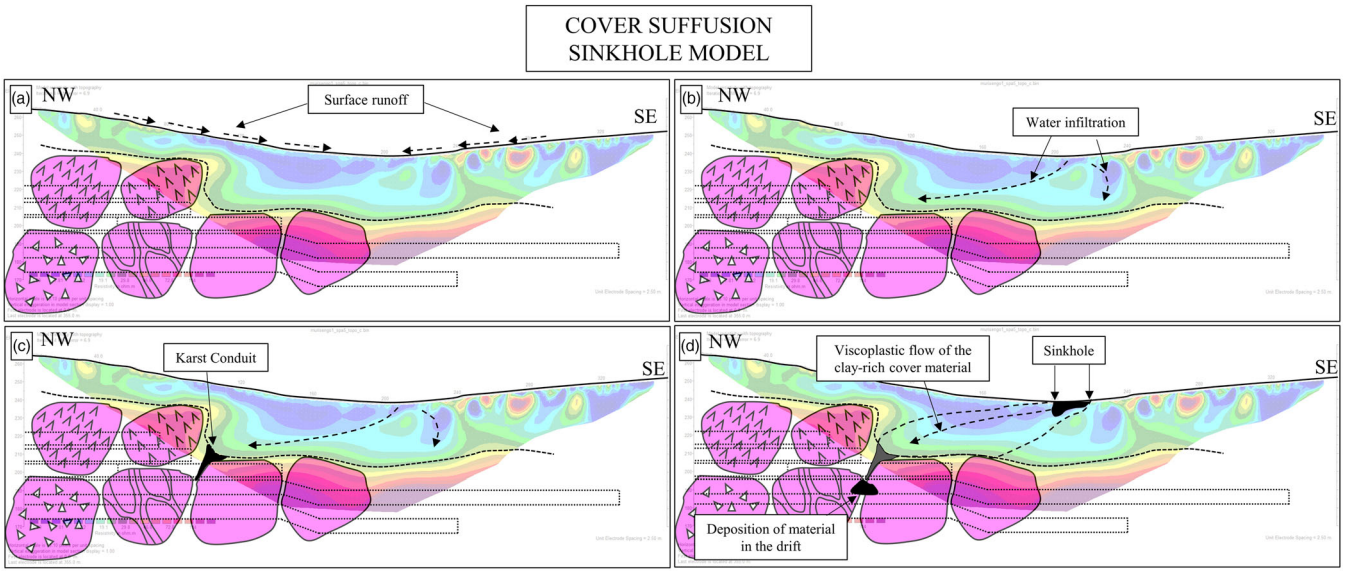

FIGURE 7 Cover suffusion model for the genesis of Murisengo sinkhole. (a) Surface runoff and water accumulation in correspondence with the position where the sinkhole will be created. (b) Water infiltration in the cover sediments. (c) Concentration of infiltered water in correspondence with a depression of the roof of the gypsum body and opening of a karst conduit. (d) Water saturation of the clay-rich cover sediments that slowly flow through the karst conduit.

10969837, 0, Downloaded from https://onlinelibrary.wiley.com/doi/10.1002/esp.5584 by CochraneItalia, Wiley Online Library on [07/05/2023]. See the Terms and Conditions (https://onlinelibrary.wiley.com/terms-and-conditions) on Wiley Online Library for rules of use; OA articles are governed by the applicable Creative Commons License

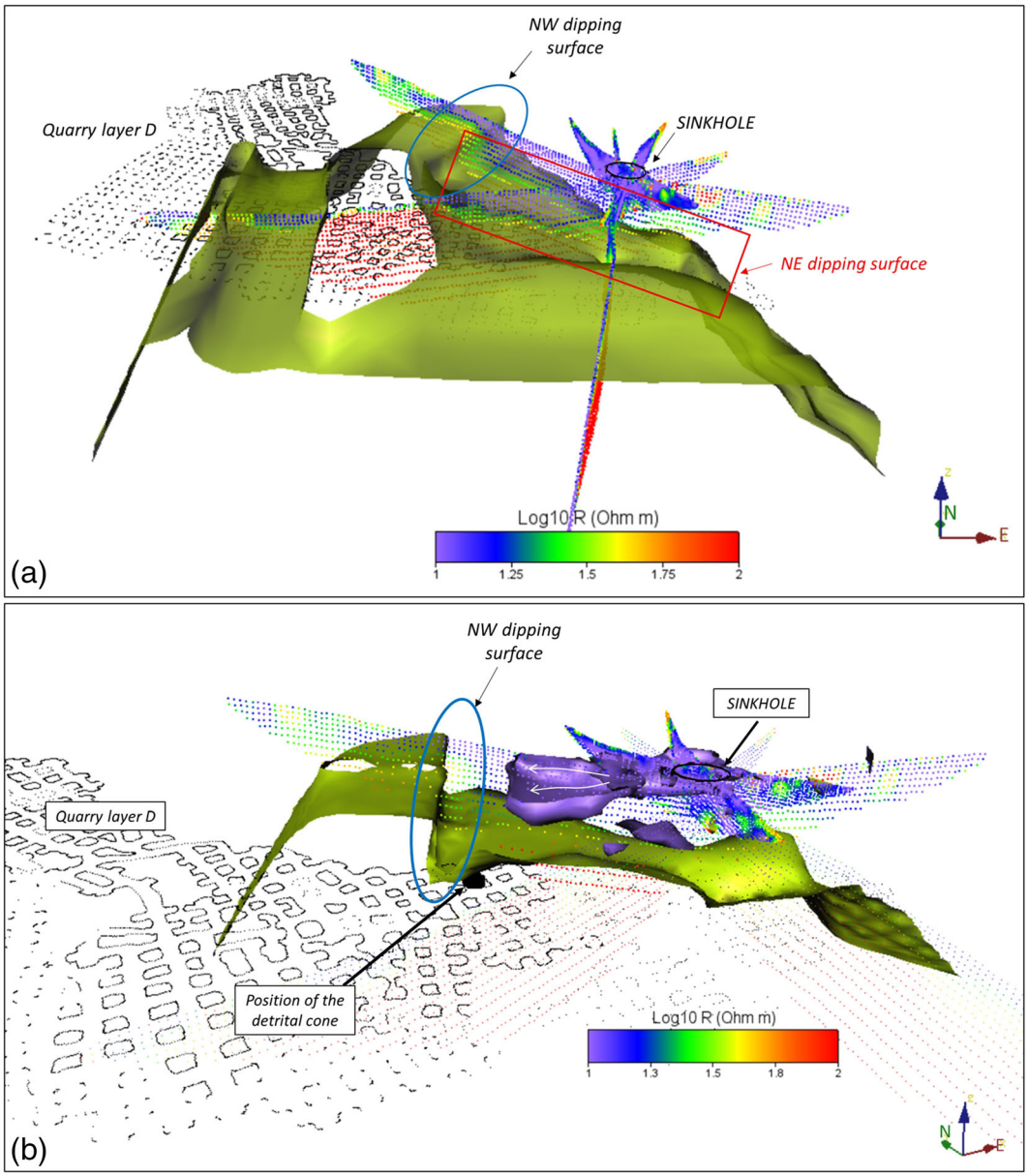

FIGURE 8 (a) 3D imaging of ERT data. The yellow surface that represents the contact between the gypsum orebody and the clay-rich sedimentary cover identifies a main dipping towards the NE (red square) and the presence of a NW-dipping structure (blue oval). The position of the sinkhole, of the ERT profiles and of the quarry layer D is reported. (b) Detail of 3D imaging of ERT data with focus on the NW-dipping structure identified by the upper limit of the gypsum volume (yellow surface). The violet surface represents the potential volume of cover sediments involved in the viscoplastic flow (white arrows). The position of the sinkhole, of the ERT profiles, of the quarry layer D and of the detrital cone is reported.

In addition to the yellow one, Figure 8b reports a second electrical resistivity isosurface (violet surface) that defines the volume of water-saturated material involved in the viscoplastic flow (white arrows). The position and orientation of the latter is consistent with the marked lateral spreading in the NW direction, revealed by the relative position of the sinkhole at the surface and the detrital cone found in the underground drift D.

Figure 9 offers additional elements supporting the hypothesis of the cover suffusion genesis of the sinkhole. Figure 9a represents the slope map of the study area, which highlights the topographical depression previously hypothesized as a possible initiation factor in sinkhole generation. As suggested by the lines of potential drainage paths of the superficial hydrographical pattern (red arrows), the sinkhole is located in a natural depression that collects a huge amount of water during rain events (considering the low permeability of the covering soils). Figure 9b reports the ERT contour lines, defined at the altitude of the sinkhole ($z = 237$ m a.s.l.). As can be seen, the contours clearly define potential flow paths within the cover sediments in the direction of the detrital cone found in the underground layer (red arrows).

Eventually, the ERT contour lines defined at the depth of the underground tunnel D of the quarry ($z = 183$ m a.s.l.; Figure 9c) show that the maximum dipping direction of the roof of the gypsum body is consistent with an accumulation of filtered water in correspondence with the position of the detrital cone (red arrows). In this position the gypsum body is strongly heterogeneous and presents a higher

10969837, 0, Downloaded from https://onlinelibrary.wiley.com/doi/10.1002/esp.5584 by CochraneItalia, Wiley Online Library on [07/05/2023]. See the Terms and Conditions (https://onlinelibrary.wiley.com/terms-and-conditions) on Wiley Online Library for rules of use; OA articles are governed by the applicable Creative Commons License

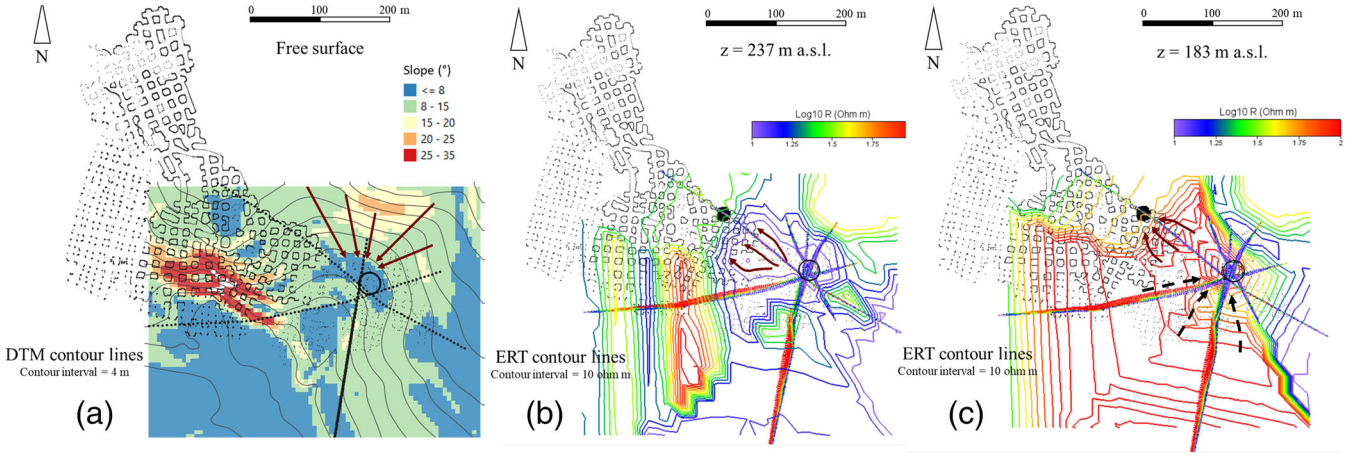

FIGURE 9 (a) Digital elevation model (contoured and slope mapping). Potential drainage paths of the superficial hydrographical pattern are identified by the red arrows. (b) Contour lines of the 3D ERT imaging at the altitude of the sinkhole. The red arrows identify potential flow directions for the viscoplastic flow. (c) Contour lines of the 3D ERT imaging at the altitude of the D underground layer. The black and red arrows identify the dip direction of the roof of the gypsum orebody in different positions. All the contour maps are overlaid on the map of the underground layer D of the quarry. The black open circle represents the position of the sinkhole, while the black closed circle represents the position of the cone of detrital material found in the tunnel.

proportion of fine matrix and inclusions with different composition (see Figure 5b) that facilitate a localization of water dissolution on gypsum and/or extrusion processes on clay. The presence of a NW-dipping discontinuity (as shown in Figure 8) becomes a preferential path of dissolution, opening the conduit (or just rearranging the particles in the fine matrix of the chaotic body) and causing the migration of covering material.

6 | CONCLUSION

A multidisciplinary investigation for sinkhole phenomenon characterization was developed by integrating geological and geostructural field analyses and geophysical surveys. Outcomes from the different approaches were combined to obtain a genetical interpretation of the process. Results suggest that the sinkhole investigated developed due to a cover suffusion process as a consequence of water accumulation within a topological depression. The meteoric water infiltered in the cover sediments reached the gypsum orebody, opening a conduit along a discontinuity. The water-saturated covering material migrated as a viscoplastic flow through the conduit, depositing the material in the drift of the underground quarry and developing the sinkhole at the surface.

The identification of the genetical mechanism of the presented case study is crucial for the interpretation and description of similar phenomena in the area, contributing to the assessment and management of sinkhole risk. The Monferrato area has a high susceptibility to sinkhole and subsidence phenomena, due to the presence of large volumes of gypsum orebodies and quarry activities.

The goodness of the obtained results confirms the applicability of ERT methods for sinkhole characterization and proposes a methodological approach that may also be useful in different contexts. There is therefore a need to increase the number of case histories discussing the application of ERT to the characterization of sinkhole phenomena in order to increase the potential of this investigation method in this context.

AUTHOR CONTRIBUTIONS

Conceptualization: Sabrina Maria Rita Bonetto, Chiara Caselle, Cesare Comina and Federico Vagnon. *Funding acquisition*: Sabrina Maria Rita Bonetto. *Methodology (including methodological development)*: Chiara Caselle and Federico Vagnon. *Investigation (e.g., data collection)*: Sabrina Maria Rita Bonetto, Chiara Caselle, Cesare Comina and Federico Vagnon. *Software (its provision and development)*: Cesare Comina and Federico Vagnon. *Writing—initial draft*: Chiara Caselle and Federico Vagnon. *Writing—reviewing and editing*: Sabrina Maria Rita Bonetto and Cesare Comina.

ACKNOWLEDGEMENTS

We thank Estrazione Gesso snc for providing access to the underground quarry and funding this research. We also acknowledge Ms. Mary Ann Mcintosh from the Language Centre (CLA) of the Politecnico di Torino for her help with English editing. Open Access Funding provided by Universita degli Studi di Torino within the CRUI-CARE Agreement.

DATA AVAILABILITY STATEMENT

Data available on request from the authors.

ORCID

Chiara Caselle https://orcid.org/0000-0002-3081-1555

REFERENCES

Al-Halbouni, D., Holohan, E.P., Taheri, A., Watson, R.A., Polom, U., Schöpfer, M.P.J., et al. (2019) Distinct element geomechanical modelling of the formation of sinkhole clusters within large-scale karstic depressions. *Solid Earth*, 10(4), 1219–1241. Available from: https://doi.org/10.5194/se-10-1219-2019

Argentieri, A., Carluccio, R., Cecchini, F., Chiappini, M., Ciotoli, G., De Ritis, R., et al. (2015) Early stage sinkhole formation in the Acque Albule basin of central Italy from geophysical and geochemical observations. *Engineering Geology*, 191, 36–47. Available from: https://doi.org/10.1016/j.enggeo.2015.03.010

Banzato, C., Vigna, B., Fiorucci, A. & De Waele, J. (2017) Hypogene gypsum caves in Piedmont (N-Italy). In: Klimchouk, A., Palmer, A.N., De

10969837, 0, Downloaded from https://onlinelibrary.wiley.com/doi/10.1002/esp.5584 by CochraneItalia, Wiley Online Library on [07/05/2023]. See the Terms and Conditions (https://onlinelibrary.wiley.com/terms-and-conditions) on Wiley Online Library for rules of use; OA articles are governed by the applicable Creative Commons License

Waele, J., Auler, A.S. & Audra, P. (Eds.) *Hypogene Karst Regions and Caves of the World*. Cham: Springer International, pp. 211–224. https://doi.org/10.1007/978-3-319-53348-3_13

Bonetto, S., Fiorucci, A., Fornaro, M. & Vigna, B. (2008) Subsidence hazards connected to quarrying activities in a karst area: the case of the Moncalvo sinkhole event (Piedmont, NW Italy). *Estonian Journal of Earth Sciences*, 57(3), 125. Available from: https://doi.org/10.3176/earth.2008.3.01

Cahalan, M.D. & Milewski, A.M. (2018) Sinkhole formation mechanisms and geostatistical-based prediction analysis in a mantled karst terrain. *Catena*, 165, 333–344. Available from: https://doi.org/10.1016/j.catena.2018.02.010

Caselle, C., Baud, P., Kushnir, A.R.L., Reuschlé, T. & Bonetto, S.M.R. (2022) Influence of water on deformation and failure of gypsum rock. *Journal of Structural Geology*, 163, 104722. Available from: https://doi.org/10.1016/j.jsg.2022.104722

Clay, R.B. & Takacs, A.P. (1997). Anticipating the unexpected—flood, fire overbreak, inrush, collapse. Paper presented at Tunnelling Under Difficult Conditions and Rock Mass Classification: Proceedings of One-Day Seminar and International Conference, 27–29 October, Basel, Switzerland.

Coli, M., Piccini, L. & Muscedra, M.M. (2020) Tunneling and karst systems: a review. In: *Rock Mechanics for Natural Resources and Infrastructure Development: Proceedings of the 14th International Congress on Rock Mechanics and Rock Engineering*. London: Taylor and Francis Group, pp. 504–511.

Dahm, T., Heimann, S. & Bialowons, W. (2011) A seismological study of shallow weak micro-earthquakes in the urban area of Hamburg city, Germany, and its possible relation to salt dissolution. *Natural Hazards*, 58(3), 1111–1134. Available from: https://doi.org/10.1007/s11069-011-9716-9

Day, M.J. (2004) Karstic problems in the construction of Milwaukee's deep tunnels. *Environmental Geology*, 45(6), 859–863. Available from: https://doi.org/10.1007/s00254-003-0945-4

De Waele, J., Gutiérrez, F., Parise, M. & Plan, L. (2011) Geomorphology and natural hazards in karst areas: a review. *Geomorphology*, 134(1–2), 1–8. Available from: https://doi.org/10.1016/j.geomorph.2011.08.001

Dela Pierre, F., Piana, F., Boano, P., Fioraso, G., Forno, M.G., Polino, R., et al. (2003) *Note Illustrative della Carta Geologica d'Italia alla scala 1: 50.000, Foglio 157 Trino*. ISPRA.

Dela Pierre, F., Natalicchio, M., Lozar, F., Bonetto, S., Carnevale, G., Cavagna, S., et al. (2016) The northernmost record of the Messinian salinity crisis (Piedmont basin, Italy). *Geological Field Trips*, 8(2.1), 58. Available from: https://doi.org/10.3301/GFT.2016.03

Galve, J., Lucha, P., Bonachea, J. & Castañeda, C. (2011) Integrating geomorphological mapping, InSAR, GPR and trenching for the identification and investigation of buried sinkholes in the mantled evaporite karst of the Ebro Valley (NE Spain). *Geomorphology*, 134(1–2), 144–156.

Gökkaya, E., Gutiérrez, F., Ferk, M. & Görüm, T. (2021) Sinkhole development in the Sivas gypsum karst, Turkey. *Geomorphology*, 386, 107746. Available from: https://doi.org/10.1016/j.geomorph.2021.107746

Golian, M., Teshnizi, E.S., Parise, M., Terzić, J., Milanović, S., Vakanjac, V.R., et al. (2021) A new analytical method for determination of discharge duration in tunnels subjected to groundwater inrush. *Bulletin of Engineering Geology and the Environment*, 80(4), 3293–3313. Available from: https://doi.org/10.1007/s10064-021-02140-6

Goodings, D.J. & Abdulla, W.A. (2002) Stability charts for predicting sinkholes in weakly cemented sand over karst limestone. *Engineering Geology*, 65(2–3), 179–184. Available from: https://doi.org/10.1016/S0013-7952(01)00127-2

Gutiérrez, F., Benito-Calvo, A., Carbonel, D., Desir, G., Sevil, J., Guerrero, J., et al. (2019) Review on sinkhole monitoring and performance of remediation measures by high-precision leveling and terrestrial laser scanner in the salt karst of the Ebro Valley, Spain. *Engineering Geology*, 248, 283–308. Available from: https://doi.org/10.1016/j.enggeo.2018.12.004

Gutiérrez, F., Cooper, A.H. & Johnson, K.S. (2008) Identification, prediction, and mitigation of sinkhole hazards in evaporite karst areas. *Environmental Geology*, 53(5), 1007–1022. Available from: https://doi.org/10.1007/s00254-007-0728-4

Gutiérrez, F., Guerrero, J. & Lucha, P. (2008) A genetic classification of sinkholes illustrated from evaporite paleokarst exposures in Spain. *Environmental Geology*, 53(5), 993–1006. Available from: https://doi.org/10.1007/s00254-007-0727-5

Gutiérrez, F., Parise, M., De Waele, J. & Jourde, H. (2014) A review on natural and human-induced geohazards and impacts in karst. *Earth-Science Reviews*, 138, 61–88. Available from: https://doi.org/10.1016/j.earscirev.2014.08.002

Hou, T., Yang, X., Xing, H., Huang, K. & Zhou, J. (2016) Forecasting and prevention of water inrush during the excavation process of a diversion tunnel at the Jinping II Hydropower Station, China. *SpringerPlus*, 5(1), 700. Available from: https://doi.org/10.1186/s40064-016-2336-9

Jia, L., Li, L., Meng, Y., Wu, Y., Pan, Z. & Yin, R. (2018) Responses of cover-collapse sinkholes to groundwater changes: a case study of early warning of soil cave and sinkhole activity on Datansha Island in Guangzhou, China. *Environmental Earth Sciences*, 77(13), 488. Available from: https://doi.org/10.1007/s12665-018-7603-3

Kaufmann, G., Gabrovšek, F. & Romanov, D. (2014) Deep conduit flow in karst aquifers revisited. *Water Resources Research*, 50(6), 4821–4836. Available from: https://doi.org/10.1002/2014WR015314

Land, L. (2013) Geophysical records of anthropogenic sinkhole formation in the Delaware Basin region, Southeast New Mexico and West Texas, USA. *Carbonates and Evaporites*, 28(1–2), 183–190. Available from: https://doi.org/10.1007/s13146-013-0126-9

Loke, M.H. (2010) Res2Dinv ver. 3.59 for Windows XP/Vista/7.

Luu, L.-H., Noury, G., Benseghier, Z. & Philippe, P. (2019) Hydro-mechanical modeling of sinkhole occurrence processes in covered karst terrains during a flood. *Engineering Geology*, 260, 105249. Available from: https://doi.org/10.1016/j.enggeo.2019.105249

Milanovic, P. (2002) The environmental impacts of human activities and engineering constructions in karst regions. *Episodes: Journal of International Geoscience*, 25(1), 13–21. Available from: https://doi.org/10.18814/epiiugs/2002/v25i1/002

Nam, B.H., Kim, Y.J. & Youn, H. (2020) Identification and quantitative analysis of sinkhole contributing factors in Florida's karst. *Engineering Geology*, 271, 105610. Available from: https://doi.org/10.1016/j.enggeo.2020.105610

Parise, M. (2010) The impacts of quarrying in the Apulian karst (Italy). In: Andreo, B., Carrasco, F., Durán, J.J. & LaMoreaux, J.W. (Eds.) *Advances in Research in Karst Media, Environmental Earth Sciences*. Berlin: Springer, pp. 441–447. https://doi.org/10.1007/978-3-642-12486-0_68

Perrin, J., Cartannaz, C., Noury, G. & Vanoudheusden, E. (2015) A multi-criteria approach to karst subsidence hazard mapping supported by weights-of-evidence analysis. *Engineering Geology*, 197, 296–305. Available from: https://doi.org/10.1016/j.enggeo.2015.09.001

Perrotti, M., Lollino, P., Fazio, N.L. & Parise, M. (2019) Stability charts based on the finite element method for underground cavities in soft carbonate rocks: validation through case-study applications. *Natural Hazards and Earth System Sciences*, 19(10), 2079–2095. Available from: https://doi.org/10.5194/nhess-19-2079-2019

Pueyo Anchuela, Ó., López Julián, P., Casas Sainz, A.M., Liesa, C.L., Pocoví Juan, A., Ramajo Cordero, J., et al. (2015) Three dimensional characterization of complex mantled karst structures: decision making and engineering solutions applied to a road overlying evaporite rocks in the Ebro Basin (Spain). *Engineering Geology*, 193, 158–172. Available from: https://doi.org/10.1016/j.enggeo.2015.04.022

Varnavina, A.V., Khamzin, A.K., Kidanu, S.T. & Anderson, N.L. (2019) Geophysical site assessment in karst terrain: a case study from southwestern Missouri. *Journal of Applied Geophysics*, 170, 103838. Available from: https://doi.org/10.1016/j.jappgeo.2019.103838

Vigna, B., D'Angeli, I., Fiorucci, A. & Waele, J.D. (2017) Hydrogeological flow in gypsum karst areas: some examples from northern Italy and main circulation models. *International Journal of Speleology*, 46(2),

10969837, 0, Downloaded from https://onlinelibrary.wiley.com/doi/10.1002/esp.5584 by CochraneItalia, Wiley Online Library on [07/05/2023]. See the Terms and Conditions (https://onlinelibrary.wiley.com/terms-and-conditions) on Wiley Online Library for rules of use; OA articles are governed by the applicable Creative Commons License

205–217. Available from: https://doi.org/10.5038/1827-806X.46.2.2095

Vigna, B., Fioraso, G., Banzato, C. & De Waele, J. (2010) Evolution of karst in Messinian gypsum (Monferrato, Northern Italy). *Geodinamica Acta*, 23(1–3), 29–40. Available from: https://doi.org/10.3166/ga.23.29-40

Xiao, X., Gutiérrez, F. & Guerrero, J. (2020) The impact of groundwater drawdown and vacuum pressure on sinkhole development: physical laboratory models. *Engineering Geology*, 279, 105894. Available from: https://doi.org/10.1016/j.enggeo.2020.105894

Youssef, A.M., Zabramwi, Y.A., Gutiérrez, F., Bahamil, A.M., Otaibi, Z.A. & Zahrani, A.J. (2020) Sinkholes induced by uncontrolled groundwater withdrawal for agriculture in arid Saudi Arabia: integration of remote-sensing and geophysical (ERT) techniques. *Journal of Arid Environments*, 177, 104132. Available from: https://doi.org/10.1016/j.jaridenv.2020.104132

Zumpano, V., Pisano, L. & Parise, M. (2019) An integrated framework to identify and analyze karst sinkholes. *Geomorphology*, 332, 213–225. Available from: https://doi.org/10.1016/j.geomorph.2019.02.013

How to cite this article: Bonetto, S.M.R., Caselle, C., Comina, C. & Vagnon, F. (2023) Geophysical surveys for non-invasive characterization of sinkhole phenomena: A case study of Murisengo. *Earth Surface Processes and Landforms*, 1–11. Available from: https://doi.org/10.1002/esp.5584

10969837, 0, Downloaded from https://onlinelibrary.wiley.com/doi/10.1002/esp.5584 by CochraneItalia, Wiley Online Library on [07/05/2023]. See the Terms and Conditions (https://onlinelibrary.wiley.com/terms-and-conditions) on Wiley Online Library for rules of use; OA articles are governed by the applicable Creative Commons License